

# NONLINEAR ANALYSIS OF LATERALLY LOADED ELASTICALLY SUPPORTED LAMINATED UNITS

**Kamel Sayed Kandil**

Civil Engng. Dept., Faculty of Engng.,  
Menofia Univ., Egypt.

**Mohammed Ibraheem El-Naggar**

Structural Engng. Dept., Faculty of Engng.,  
Alex. Univ., Alexandria, Egypt.

**Mohammed Abd El-Khalik Sakr**

Civil Engng. Dept., Faculty of Engng.,  
Tanta Univ., Egypt.

## ABSTRACT

Behavior of laminated unit depends mainly on the material of the plates as well as the shear modulus of the interlayer. Several unknowns face the designer who is considering the use of laminated units in engineering applications. The designer has little authoritative resources that provide insight into the structural mechanics of laminated units. The present work is aimed at developing a mathematical model for the nonlinear analysis of laterally loaded rectangular laminated units resting on elastic supports. Using variational calculus and the principle of minimum potential energy five nonlinear differential equations with appropriate boundary conditions are obtained. These equations are solved numerically using the finite difference method with an iteration routine. The present model is used to provide an insight into the stress pattern at the linear and nonlinear stages of the behavior of laterally loaded laminated unit having different degrees of interlayer shear modulus.

## INTRODUCTION

Laminated unit consists of two (or more) monolithic plates glued together by an elastomeric material to form one unit. Laminated glass units are used in a variety of products to resist a wide range of loading and environmental conditions. Included are architectural glazing products such as insulating glass, overhead glazing, and safety glazing. There are two principal advantages of laminated glass over monolithic plate. First, the material properties of architectural laminates are such that when glass fracture occurs, the individual fragments remain adhered to the plastic interlayer and complete collapse of the glazed member is prevented. Secondly, architectural laminates are constructed in such a way that they can be effectively employed in the control of shading and solar heat gain in buildings.

With larger sizes of thin plates being subjected to lateral loads, the maximum lateral displacement of the plate can exceed several times the thickness of the plate. When the maximum lateral deflection exceeds about 75% of the plate thickness, linear theories are not useful, where membrane stresses are developed in the plate in addition to bending stresses. A nonlinear

plate theory was developed by von Karman [1] in 1910. He coupled the effect of in-plane force with out-of-plane deflection by using the principle of minimum potential energy and applying the Euler equation. Closed form solution for von Karman theory, even for simple square plate, is not known. With the help of digital computers numerical techniques such as finite difference and finite element are developed to solve von Karman equations.

## PREVIOUS WORK ON LAMINATED PLATES

In an early work, Hoff [2,3] derived the differential equation of sandwich beams subjected to lateral and in-plane loading using the principle of virtual displacement. His results have been shown to agree well with his own experimental results. Based on the assumption that plane section for the whole sandwich plate system before bending remains plane after bending, Reissner [4] in 1948 and Wang [5] in 1952 developed equations for finite deflection of sandwich plate. They considered the transverse deformation and compressibility of the inner core but neglected the

bending resistance of the face plates. Reissner theory is not applicable to laminated glass problem since it was derived for a thick core as compared to the two plates.

Hooper [6] in 1973 performed theoretical and experimental research on the bending resistance of laminated glass beams. He found that the bending resistance of these beams depends primarily upon the thickness and shear modulus of the interlayer. Thicker interlayers were observed to demonstrate lower effective shear moduli than thinner interlayers of the same material. Furthermore, the effective shear modulus of the interlayer was found to be inversely proportional to plasticizer content, ambient temperature, and duration of loading. Hooper concluded that for sustained load (*e.g.*, snow and self weight) laminated units should be considered as two independent glass layers, with no coupling effect due to the interlayer. For wind loading, glass bending stress may be estimated on the basis of an interlayer shear modulus corresponding to the maximum temperature at which such loading is likely to occur, due to solar radiation effect. Hooper's conclusions are based on evaluation of the behavior of small scale beams [2x10x0.8 in. (50.8x254x16 mm)].

Behr, *et al.* [7] in 1985, due to lack of mathematical model for analysis of laminated glass units, compared the behavior of laminated plate to that of layered plate (without interlayer) and monolithic plate having the same size and thickness. The experimental data revealed that the behavior of laminated plate was closer to that of the monolithic behavior at ordinary temperature. At higher temperature, the interlayer softens and the behavior becomes closer to that of layered plate.

Reznik and Minor [8] in 1986 and Linden, *et al.* [9] in 1988 conducted extensive experimental study on the load deformation characteristic and strength of laminated glass units as compared to their monolithic counterpart. Reznik and Minor concluded that larger strength-factor values than those adopted by model building codes [10, 11, 12] may be justified, at least for loading conditions in which short-duration loads (*e.g.*, wind load) occur at temperatures below about 49°C. (The relative strength factor is the ratio of the strength of laminated glass relative to the strength of monolithic glass. This factor is less than one.)

Das and Vallabhan [13] in 1988 developed a

sophisticated mathematical model for the nonlinear analysis and structural behavior of sandwich plates where they took into consideration the transverse shear deformation as well as the compressibility of the core. Their model is only among the previous models theoretically applicable to the nonlinear analysis of laminated plates since the assumptions used agree with the mechanics of the problem as observed in experiments. However, their model is too complex and has not been formulated numerically.

Later, Vallabhan, *et al.* [14] in 1991, using the variational principle and von Karman assumptions for large deflection of plates developed a more simplified mathematical model. They show that the classical assumption, that plane section for the whole unit before deformation remains plane after deformation, becomes nonrealistic. They assumed a more realistic assumption that plane section before deformation remains plane after deformation for each individual plate and that the interlayer transmits certain amount of shear between the two glass plates. Their model is limited to simply supported boundary conditions.

Rarely, is perfect fixity attained along the boundaries of a plate and the boundaries should in reality be considered to possess varying degrees of in-plane displacement restraint, out-of-plane displacement restraint and rotational restraint in the lateral direction. The aim of the present work is to establish a mathematical model capable of analyzing laminated plates resting on elastic supports along their boundaries. Here, the laminated unit is assumed to be resting on two translational springs and one rotational spring as shown in Figure (1). The translational springs act in the in-plane and the out-of-plane directions. The rotational spring resists the plate rotation in the lateral direction along its edges. The present model is used to provide an insight into the behavior of structurally glazed architectural laminated glass units. This model is an extension to the work done by Vallabhan *et al.* [14].

## THE MATHEMATICAL MODEL

The mathematical model is based on the concept of minimum total potential energy of the plates and interlayer of the laminated glass unit. The plates have different thicknesses and will have both bending and membrane strain energies, whereas the interlayer

will have only shear strain energy. Since the plates are bonded together, there is continuity of displacement at the interfaces and plane sections remain plane in the individual components, but not for the entire composite. All assumptions made in the von Karman nonlinear theory of plates are used for modelling the glass plates. Since the thickness of the interlayer is relatively small its compressibility is neglected and only the shear strain energy in the interlayer is considered.

The total potential energy  $V$  of the laminated unit can be expressed as:

$$V = \bar{U}_m^{(1)} + \bar{U}_b^{(1)} + \bar{U}_m^{(2)} + \bar{U}_b^{(2)} + \bar{U}_{xz}^{(I)} + \bar{U}_{yz}^{(I)} + \bar{\Omega} \quad (1)$$

here  $\bar{U}_m^{(i)}$  and  $\bar{U}_b^{(i)}$  are the membrane and bending strain energies of plate ( $i$ ); respectively, where  $i = 1, 2$  for top and bottom plates; respectively. Also,  $\bar{U}_{xz}^{(I)}$  and  $\bar{U}_{yz}^{(I)}$  are the shear strain energies of the interlayer due to the shear strains  $\gamma_{xz}^{(I)}$  and  $\gamma_{yz}^{(I)}$ ; respectively and  $\bar{\Omega}$  is the potential energy function due to the applied loads.

*Strain Energy Function of the Plates*

The membrane energy function of the plate can be expressed in terms of the strain in the plate as:

$$\bar{U}_m^{(i)} = \int_{(-b/2)}^{(+b/2)} \int_{(-a/2)}^{(+a/2)} U_m^{(i)} dx dy \quad (2)$$

$$\bar{U}_m^{(i)} = \int_{(-b/2)}^{(+b/2)} \int_{(-a/2)}^{(+a/2)} \frac{Eh_i}{2(1-\nu^2)} [e_{ix}^2 + e_{iy}^2 + 2\nu e_{ix}e_{iy} + \frac{1}{2}(1-\nu)e_{ixy}^2] dx dy \quad (3)$$

where  $h_i$  denotes thickness of the plate ( $i$ ),  $a$  and  $b$  are the lengths of the plate in the  $x$  and  $y$  directions; respectively and  $i = 1, 2$  denotes the top and bottom plates; respectively. The subscript "comma" notation represents differentiation with respect to the variables following it.

Similarly, the bending strain energy function is expressed as:

$$\bar{U}_b^{(i)} = \int_{(-b/2)}^{(+b/2)} \int_{(-a/2)}^{(+a/2)} U_b^{(i)} dx dy \quad (4)$$

$$U_m^{(i)} = \int_{(-b/2)}^{(+b/2)} \int_{(-a/2)}^{(+a/2)} \frac{Eh_i^3}{24(1-\nu^2)} [w_{,xx}^2 + w_{,yy}^2 + 2\nu w_{,xx}w_{,yy} + 2(1-\nu)w_{,xy}^2] dx dy \quad (5)$$

*Strain Energy Function of the Interlayer*

For the interlayer, Figure (2), the average shear strain,  $\gamma_{xz}$  is given as:

$$\gamma_{xz} = \phi + \theta = -w_{,x} + u_{,z}$$

$$\gamma_{xz} = \left[ u_1 - u_2 - w_{,x} \left( \frac{h_1}{2} + \frac{h_2}{2} + t \right) \right] / t \quad (6)$$

where  $t$  is the thickness of the interlayer. Similarly,

$$\gamma_{yz} = \left[ v_1 - v_2 - w_{,y} \left( \frac{h_1}{2} + \frac{h_2}{2} + t \right) \right] / t \quad (7)$$

Making use of Eqs. (6) and (7), the interlayer shear strain energy expressions are given as:

$$\bar{U}_{xz}^{(I)} = \int_{(-b/2)}^{(+b/2)} \int_{(-a/2)}^{(+a/2)} U_{xz}^{(I)} dx dy = \int_{(-b/2)}^{(+b/2)} \int_{(-a/2)}^{(+a/2)} \frac{1}{2} G_I \gamma_{xz}^2 dx dy \quad (8)$$

$$\bar{U}_{xz}^{(I)} = \int_{(-b/2)}^{(+b/2)} \int_{(-a/2)}^{(+a/2)} \frac{G_I}{2t} \left[ u_1 - u_2 - w_{,x} \left( \frac{h_1}{2} + \frac{h_2}{2} + t \right) \right]^2 dx dy \quad (9)$$

Similarly,

$$\bar{U}_{yz}^{(I)} = \int_{(-b/2)}^{(+b/2)} \int_{(-a/2)}^{(+a/2)} \frac{G_I}{2t} \left[ v_1 - v_2 - w_{,y} \left( \frac{h_1}{2} + \frac{h_2}{2} + t \right) \right]^2 dx dy \quad (10)$$

where  $G_I$  is the interlayer shear modulus.

*Potential Energy due to the Applied Load*

For the case of symmetrical lateral load,  $q$ , acting on the laminated unit, the load potential energy function  $\bar{\Omega}$  is given by:

$$\bar{\Omega} = \int_{(-b/2)}^{(+b/2)} \int_{(-a/2)}^{(+a/2)} \Omega dx dy = - \int_{(-b/2)}^{(+b/2)} \int_{(-a/2)}^{(+a/2)} q w dx dy \quad (11)$$

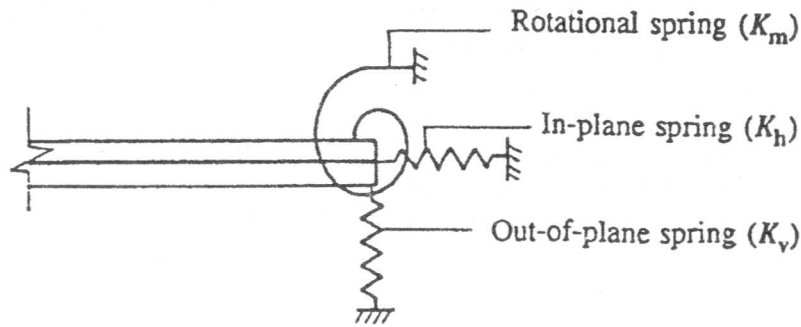


Figure 1. Types of elastic restraints along the unit edges.

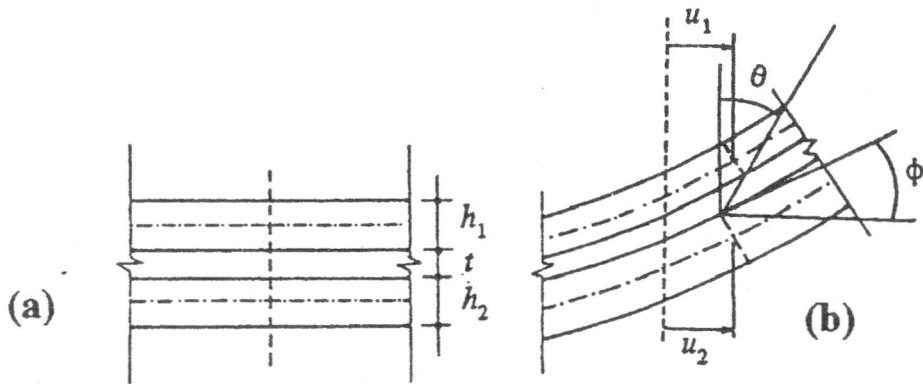


Figure 2. Laminated unit; (a) undeformed section (b) deformed section.

Substituting from Eqs. (3, 5, 9, 10 and 11) into Equ. 1, the total potential energy  $V$  of the laminated unit is given as:

$$V = \int_{(-b/2)(-a/2)}^{(+b/2)(+a/2)} [U_m^{(1)} + U_b^{(1)} + U_m^{(2)} + U_b^{(2)} + U_{xz}^{(1)} + U_{yz}^{(1)} + \Omega] dx dy \quad (12)$$

$$V = \int_{(-b/2)(-a/2)}^{(+b/2)(+a/2)} F dx dy \quad (13)$$

where,

$$F = \frac{Eh_1}{2(1-\nu^2)} [e_{1,x}^2 + e_{1,y}^2 + 2\nu e_{1,x}e_{1,y} + \frac{1}{2}(1-\nu)e_{1,xy}^2] + \frac{Eh_2}{2(1-\nu^2)} [e_{2,x}^2 + e_{2,y}^2 + 2\nu e_{2,x}e_{2,y} + \frac{1}{2}(1-\nu)e_{2,xy}^2]$$

$$+ \frac{E(h_1^3 + h_2^3)}{24(1-\nu^2)} [w_{xx}^2 + w_{yy}^2 + 2\nu w_{xx}w_{yy} + 2(1-\nu)$$

$$+ \frac{G_I}{2t} [u_1 - u_2 - w_{,x}(\frac{h_1}{2} + \frac{h_2}{2} + t)]^2$$

$$+ \frac{G_I}{2t} [v_1 - v_2 - w_{,y}(\frac{h_1}{2} + \frac{h_2}{2} + t)]^2 - q$$

Using the principle of minimum potential energy Euler equations can be obtained as:

$$\frac{\partial F}{\partial s} - \frac{\partial}{\partial x} \left[ \frac{\partial F}{\partial s_{,x}} \right] - \frac{\partial}{\partial y} \left[ \frac{\partial F}{\partial s_{,y}} \right] + \frac{\partial^2}{\partial x^2} \left[ \frac{\partial F}{\partial s_{,xx}} \right] + \frac{\partial^2}{\partial y^2} \left[ \frac{\partial F}{\partial s_{,yy}} \right] + \frac{\partial^2}{\partial y \partial x} \left[ \frac{\partial F}{\partial s_{,xy}} \right] = 0$$

where  $s$  denotes  $u_1, v_1, u_2, v_2$  and  $w$ ; respective Using Equ. (15), one gets the five equation

equilibrium governing the laminated glass plate system:

$$e_{,xy} = u_{,y} + v_{,x} + w_{,xy} \quad (21)$$

In Eqs. (16, 17, 18, 19 and 20), the left-hand side constitutes only of linear terms. Nonlinear terms in the lateral deflection  $w$  are brought to the right-hand side. This arrangement is essential for the iterative procedure discussed later in this paper.

### THE BOUNDARY CONDITIONS

The different degrees of restraints along the plate edges can be expressed in terms of three elastic springs as shown in Figure (1). In this figure  $K_v$ ,  $K_m$  and  $K_h$  represent the out-of-plane, the rotational and the in-plane spring constants along the plate boundaries; respectively. If the axes are taken as shown in Figure (3), the different boundary conditions can be expressed as:

At  $x = 0$ :

$$u_1 = u_2 = e_{1,xy} = e_{2,xy} = w_{,x} = 0 \text{ and } w_{,xxx} + (2 - \nu)w_{,xyy} = 0 \quad (22)$$

At  $x = a/2$ :

$$e_{1,xy} = 0, \quad e_{2,xy} = 0, \quad (23)$$

$$N_{1x} = \frac{Eh_1}{1 - \nu^2} (e_{1,x} + \nu e_{1,y}) = -u_1 K_h, \quad (24)$$

$$N_{2x} = \frac{Eh_2}{1 - \nu^2} (e_{2,x} + \nu e_{2,y}) = -u_2 K_h, \quad (25)$$

$$-(D_1 + D_2)[w_{,xxx} + (2 - \nu)w_{,xyy}] = -wK_v \text{ and } (26)$$

$$-(D_1 + D_2)[w_{,xx} + \nu w_{,yy}] = -w_x K_m \quad (27)$$

At  $y = 0$ :

$$v_1 = v_2 = e_{1,xy} = e_{2,xy} = w_{,y} = 0 \text{ and } w_{,yyy} + (2 - \nu)w_{,xyy} = 0 \quad (28)$$

At  $y = b/2$ :

$$e_{1,xy} = 0, \quad e_{2,xy} = 0, \quad (29)$$

$$\left[ (D_1 + D_2) \nabla^4 - \frac{G_I}{t} \left( \frac{h_1}{2} + \frac{h_2}{2} + t \right)^2 \nabla^2 \right] w = q$$

$$+ \frac{Eh_1}{1 - \nu^2} [(e_{1,x} + \nu e_{1,y})w_{,xx} + (e_{1,y} + \nu e_{1,x})w_{,yy} + (1 - \nu)e_{1,xy}w_{,xy}]$$

$$+ \frac{Eh_2}{1 - \nu^2} [(e_{2,x} + \nu e_{2,y})w_{,xx} + (e_{2,y} + \nu e_{2,x})w_{,yy} + (1 - \nu)e_{2,xy}w_{,xy}]$$

$$- \frac{G_I}{t} \left( \frac{h_1}{2} + \frac{h_2}{2} + t \right) (u_{1,x} - u_{2,x} + v_{1,y} - v_{2,y}) \quad (16)$$

$$\left[ \frac{\partial^2}{\partial x^2} + \frac{1 - \nu}{2} \frac{\partial^2}{\partial y^2} - \frac{G_I(1 - \nu)}{2Gh_1 t} \right] u_1 + \left[ \frac{1 + \nu}{2} \frac{\partial^2}{\partial x \partial y} \right] v_1 + \left[ \frac{G_I(1 - \nu)}{2Gh_1 t} \right] u_2 =$$

$$-w_{,x}(w_{,xx} + \frac{1 - \nu}{2}w_{,yy}) - \frac{1 + \nu}{2}w_{,xy}w_{,y} - \frac{G_I(1 - \nu)}{2Gh_1 t} \left( \frac{h_1}{2} + \frac{h_2}{2} + t \right) w_{,x} \quad (17)$$

$$\left[ \frac{\partial^2}{\partial y^2} + \frac{1 - \nu}{2} \frac{\partial^2}{\partial x^2} - \frac{G_I(1 - \nu)}{2Gh_1 t} \right] v_1 + \left[ \frac{1 + \nu}{2} \frac{\partial^2}{\partial x \partial y} \right] u_1 + \left[ \frac{G_I(1 - \nu)}{2Gh_1 t} \right] v_2 =$$

$$-w_{,y}(w_{,yy} + \frac{1 - \nu}{2}w_{,xx}) - \frac{1 + \nu}{2}w_{,xy}w_{,x} - \frac{G_I(1 - \nu)}{2Gh_1 t} \left( \frac{h_1}{2} + \frac{h_2}{2} + t \right) w_{,y} \quad (18)$$

$$\left[ \frac{\partial^2}{\partial x^2} + \frac{1 - \nu}{2} \frac{\partial^2}{\partial y^2} - \frac{G_I(1 - \nu)}{2Gh_2 t} \right] u_2 + \left[ \frac{1 + \nu}{2} \frac{\partial^2}{\partial x \partial y} \right] v_2 + \left[ \frac{G_I(1 - \nu)}{2Gh_2 t} \right] u_1 =$$

$$-w_{,x}(w_{,xx} + \frac{1 - \nu}{2}w_{,yy}) - \frac{1 + \nu}{2}w_{,xy}w_{,y} - \frac{G_I(1 - \nu)}{2Gh_2 t} \left( \frac{h_1}{2} + \frac{h_2}{2} + t \right) w_{,x} \quad (19)$$

$$\left[ \frac{\partial^2}{\partial y^2} + \frac{1 - \nu}{2} \frac{\partial^2}{\partial x^2} - \frac{G_I(1 - \nu)}{2Gh_2 t} \right] v_2 + \left[ \frac{1 + \nu}{2} \frac{\partial^2}{\partial x \partial y} \right] u_2 + \left[ \frac{G_I(1 - \nu)}{2Gh_2 t} \right] v_1 =$$

$$-w_{,y}(w_{,yy} + \frac{1 - \nu}{2}w_{,xx}) - \frac{1 + \nu}{2}w_{,xy}w_{,x} - \frac{G_I(1 - \nu)}{2Gh_2 t} \left( \frac{h_1}{2} + \frac{h_2}{2} + t \right) w_{,y} \quad (20)$$

where  $G$  is the shear modulus of the plate material, and  $D_1$  and  $D_2$  are the flexural rigidities of the top and bottom plates; respectively. Also,  $e_{,x}$ ,  $e_{,y}$  and  $e_{,xy}$  are the nonlinear membrane strains, which are expressed in terms of the displacements as:

$$e_{,x} = u_{,x} + \frac{1}{2}w_{,x}^2, \quad e_{,y} = v_{,y} + \frac{1}{2}w_{,y}^2 \quad \text{and}$$

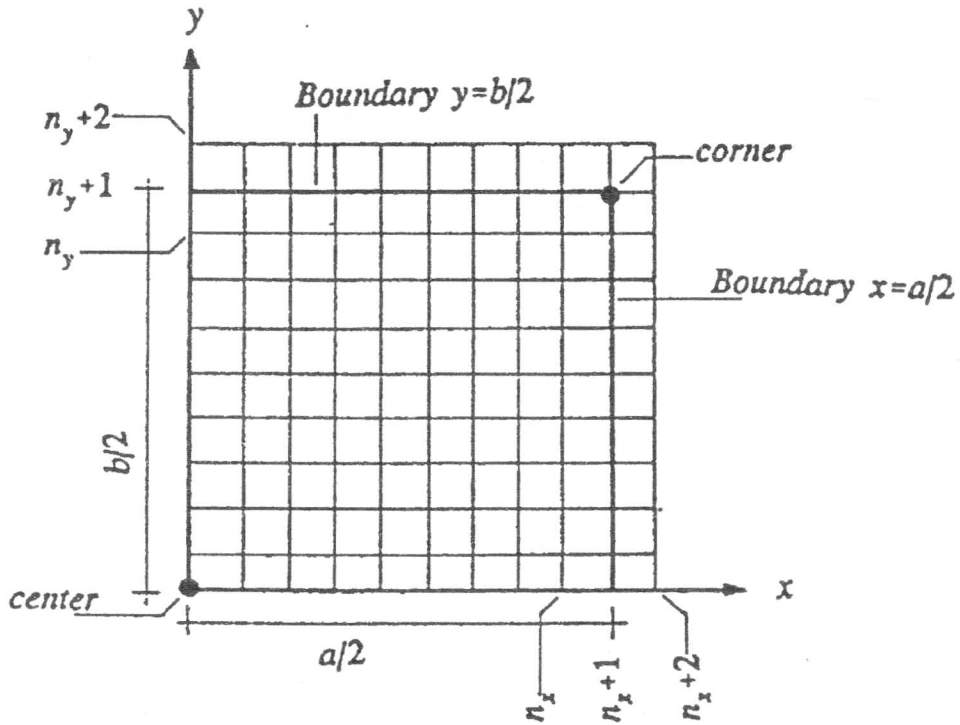


Figure 3. Finite difference mesh for in-plane displacements.

$$N_{1y} = \frac{Eh_1}{1-\nu^2}(e_{1,y} + \nu e_{1,x}) = -\nu_1 K_h, \quad (30)$$

$$N_{2y} = \frac{Eh_2}{1-\nu^2}(e_{2,y} + \nu e_{2,x}) = -\nu_2 K_h, \quad (31)$$

$$-(D_1 + D_2)[w_{,yyy} + (2-\nu)w_{,xxy}] = -wK_v \text{ and } (32)$$

$$-(D_1 + D_2)[w_{,yy} + \nu w_{,xx}] = -w_{,y}K_m \quad (33)$$

The above boundary conditions are given for a quarter plate, assuming symmetry with respect to  $x$  and  $y$  axes.

### SOLUTION TECHNIQUE

The well known central finite difference technique is used to transform the continuous functions  $u_1, u_2, v_1, v_2$  and  $w$  into discrete values at every point of the finite

difference mesh. The system of differential equations is transformed therefore into a system of algebraic equations. The terms in the left-hand side of the field and boundary equations, being linear, can be transformed into linear differential operators, while the nonlinear terms in the right-hand side are condensed into a right-hand side vector. For the lateral deflection,  $w$ , the finite difference mesh size is  $(n_x+1)(n_y+1)$  where  $n_x$  and  $n_y$  being the number of subdivisions in the  $x$  and  $y$  directions; respectively (Figure (3)). The complete finite difference model for the lateral deflection with the associated boundary conditions are given in Ref. [15].

For the in-plane displacements,  $u_1, u_2, v_1$  and  $v_2$ , the finite difference mesh size is  $(n_x + 2)(n_y + 2)$ . In addition to the edge displacements, fictitious points outside the domain are considered in the proximity of the edges of the plate (Figure (3)). At every point of the finite difference mesh, there are four unknowns  $u_2, v_1, v_2$  and four finite difference field equations written per point. Along the edges  $x = 0$  and  $y = 0$  the field equations are modified to account for

boundary conditions, while at the edges  $x = a/2$  and  $y = b/2$ , four additional boundary condition equations per point are applied, so that the total number of unknowns is equal to the number of equations. At the corner point lying at the inter-section of the plate edges, the field equations are modified and twelve independent boundary conditions are written. The total number of in-plane displacement unknowns is  $4(n_x+2)(n_y+2)$ . The finite difference equations for the in-plane displacements with the associated boundary conditions are given in Ref. [15].

The five nonlinear differential equations (Eqs. 16, 17, 18, 19 and 20) are solved using the classical finite difference method. In a matrix form, the left-hand side of the algebraic equations generated from field Eq. (16) are stored in matrix  $[A]$ , while those equations generated from Eqs. 17, 18, 19, and 20 are kept in matrix  $[B]$ . Therefore, the system of equations can be written as:

$$[A] \{W\} = \{q + f_1(w, u_1, u_2, v_1, v_2)\} \quad (34)$$

$$[B] \{U\} = \{f_2(w)\} \quad (35)$$

where  $\{W\}$  is the lateral displacement vector,  $\{U\}$  is the in-plane displacement vector, constituting of the values of  $u_1, v_1, u_2$  and  $v_2$ ; respectively, at every finite difference mesh point and  $\{q\}$  is the applied lateral load vector.

Matrix  $[A]$  is symmetric and banded; therefore only a half banded matrix is used in the solution process while matrix  $[B]$  is found to be unsymmetric when all the boundary conditions are incorporated. The iterative scheme explained below is employed in the solution process.

Since the right hand-side of Eqs. (34) and (35) are not known priori, values of  $u_1, u_2, v_1, v_2$  and  $w$  from the  $(i-1)^{th}$  iterative step are used to form the right-hand side vector of system (34) of equations for the  $i^{th}$  iteration. The new set of equation(s) at the  $i^{th}$  step become:

$$[A] \{W\}_i = \{q + f_1(w, u_1, v_1, u_2, v_2)\}_{(i-1)} \quad (36)$$

$$[B] \{U\}_i = \{f_2(w)\}_i \quad (37)$$

Equ. (36) is solved for  $\{W\}$ . The new value of  $\{W\}$  is used to calculate the right-hand side of Equ. (37) that is solved for  $\{U\}$ , i.e.,  $u_1, v_1, u_2$  and  $v_2$ . The procedure is repeated until the solution converges to a

final value for each increment of load such that, the error in  $w$  for the  $i^{th}$  iteration:

$$\epsilon^i = \frac{\sum_{j=1}^N \|w_j^i - w_j^{(i-1)}\|}{N} \leq \gamma (w_{max})^i \quad (38)$$

in which  $N$  is the total number of nodes in the grid, where  $\gamma$  is a prescribed small positive number to represent the iteration tolerance.

It is found that the above iterative scheme will converge only in the case of small deflection. When deflections become large, the scheme will diverge. By dividing the load to a number of increments and using interpolated values of the lateral displacement  $w$ , the iterative technique will converge faster to the correct solution.

### ILLUSTRATIVE EXAMPLES

#### Example 1

The purpose of this example is to study the effect of the mesh size on the accuracy of the finite difference method. Also, the effect of the spring coefficients  $K_m$  and  $K_h$  on the behavior of the unit is included in this example. The unit dimensions and properties are as follows:  $a=b=150$  cm,  $h_1=h_2=0.4$  cm,  $t=0.1$  cm,  $E=6.9 \times 10^6$  N/cm<sup>2</sup>,  $\nu=0.22$ ,  $G_1=100$  N/cm<sup>2</sup>, and  $K_v=10^{20}$  N/cm<sup>2</sup>.

**Table 1.** Maximum reached load ( $q_{max}$ ), maximum deflection ( $w_{max}$ ), maximum principal stress ( $\sigma_p$ ) and *cpu* time for different mesh sizes ( $K_m = K_h = 0$ ).

Mesh size	$q_{max}$ (N/cm <sup>2</sup> )	$w_{max}^*/w_{max}$ at max. load	$\sigma_p^*/\sigma_p$ at max. load	<i>cpu</i> time (hh:mm:ss)
5x5	0.4	0.851	0.790	00:00:35
10x10	0.8	0.940	0.878	00:06:09
12x12	0.9	0.957	0.920	00:12:58
15x15	1.0	0.982	0.977	00:25:26
18x18	> 1.0	0.990	0.984	01:10:54
20x20	> 1.0	1.000	1.000	01:51:52

$w_{max}^*$  and  $\sigma_p^*$  are the maximum deflection and maximum principal stress for (20x20) mesh size.

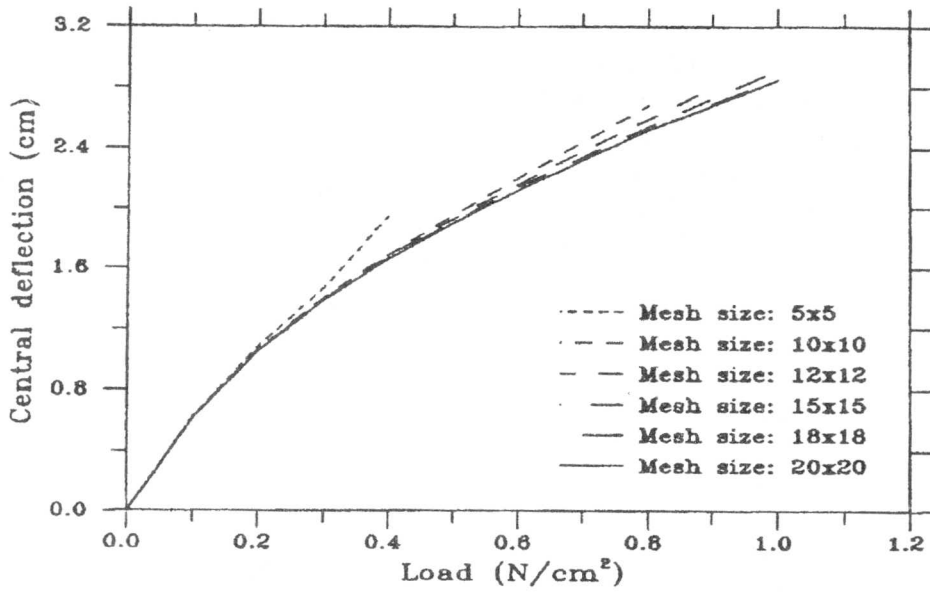


Figure 4. Central deflection vs. applied lateral load for different mesh sizes.

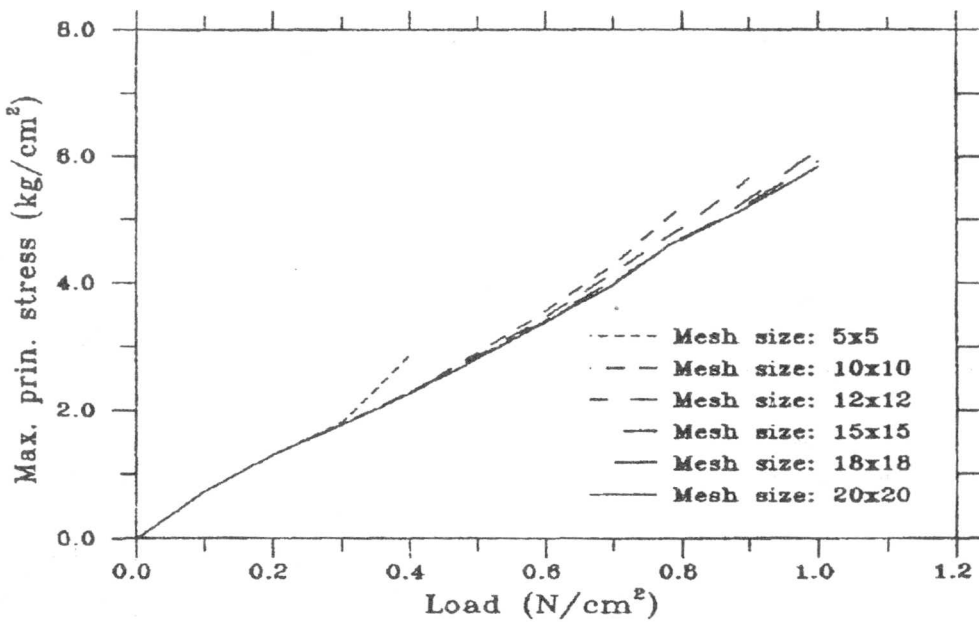
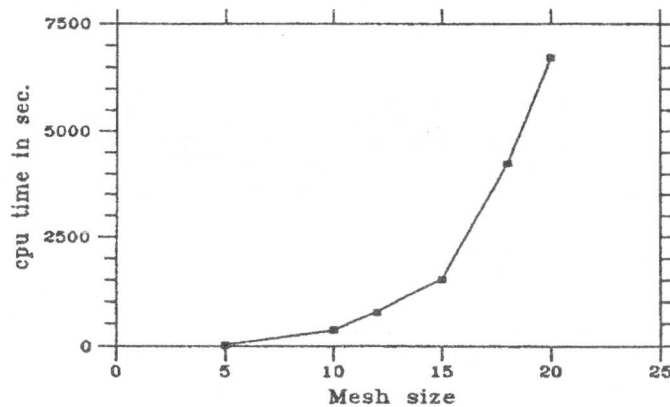
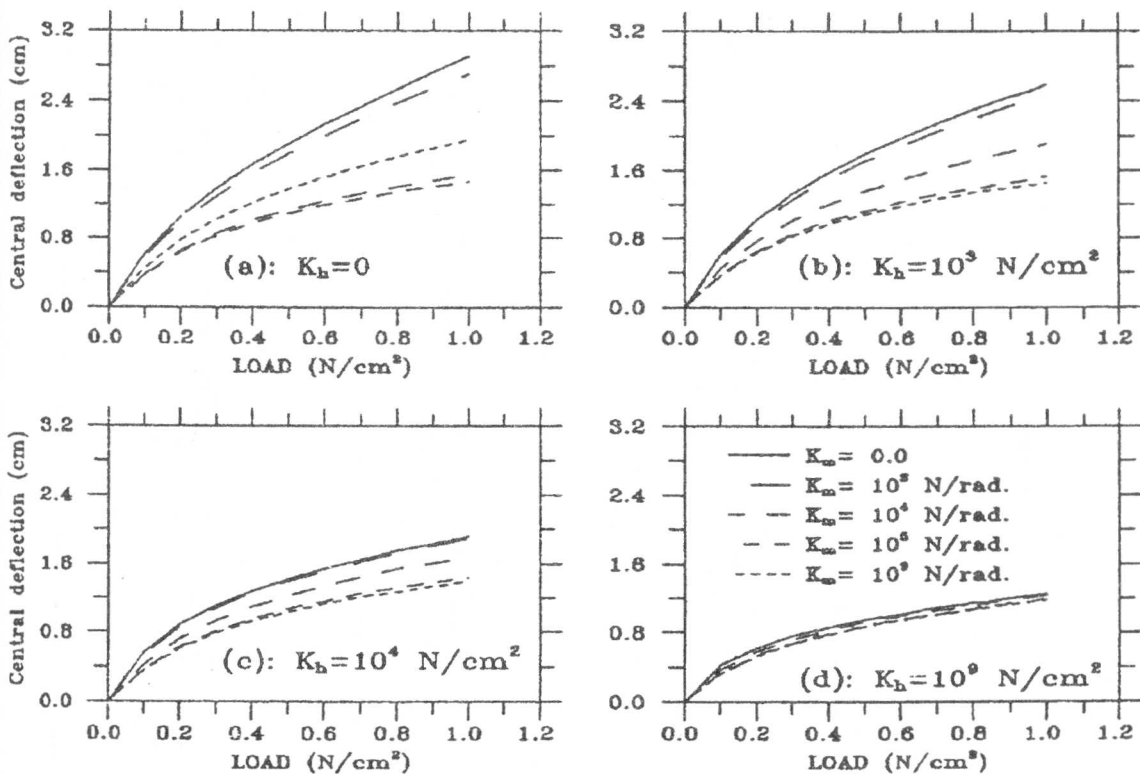


Figure 5. Maximum principal tensile stress vs. applied lateral load for different mesh size.



Figure 6. *cpu* time vs. mesh size.Figure 7. Central deflection vs. applied lateral load for different values of the spring constants  $K_m$  and  $K_h$ 

The effect of the mesh size on the accuracy of lateral deflections and maximum principal stresses are shown in Figures (4) and (5). The total computation time in seconds, *cpu time*, on Micro/Vax computer for various mesh sizes is shown in Figure (6). Finer mesh sizes lead to better convergence through load steps and hence higher load levels can be analyzed. Table (1) reports the highest load level reached through the analysis and the corresponding computation time for

the different mesh sizes. Also, included in this table are the ratios of maximum deflection and maximum principal stress of each mesh size compared to those of 20x20 mesh size. As can be seen from this table for a 15x15 mesh size, the deflection and maximum principal stress differ by about 2% of their correlatives obtained from 20x20 mesh size; however, the *cpu* time reduces, for the 15x15 mesh size, by about 77%.

Table 2. Stress distribution in the x-direction through the cross-section at the center of monolithic, layered laminated plates ( $q = 0.04 \text{ N/cm}^2$ ).

Case	$G_f$ $\text{N/cm}^2$	Section	Stresses in x-direction ( $\text{kN/cm}^2$ )		
			Bending stress	Membrane stress	Total stress
Lay.	0.0				
Lam.	50				
Lam.	100				
Lam.	130				
Mon.					

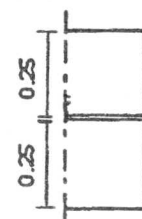

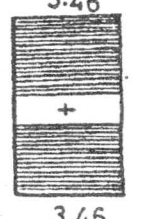

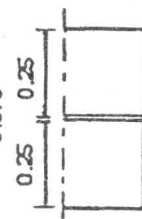

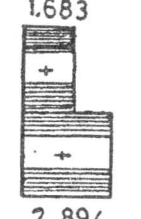

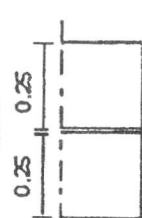
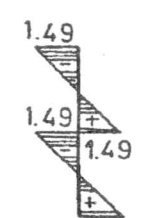
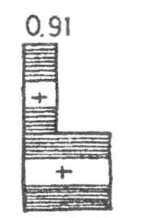
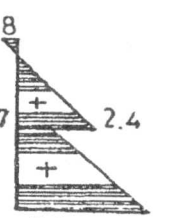
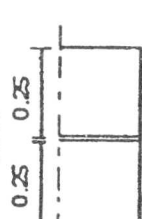
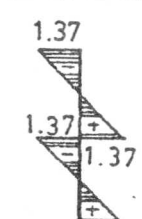
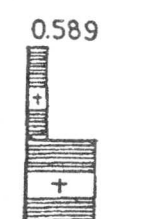
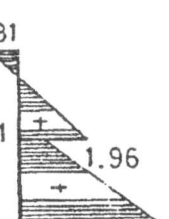
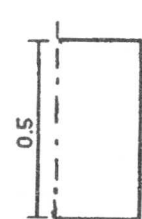
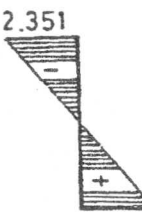
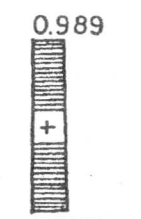
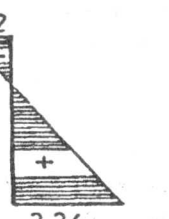
Table 3. Stress distribution in the  $x$ -direction through the cross-section at the center of monolithic, layered and laminated plates ( $q = 1.2 \text{ N/cm}^2$ ).

Case	$G_1$ N/cm <sup>2</sup>	Section	Stresses in $x$ -direction (kN / cm <sup>2</sup> )		
			Bending stress	Membrane stress	Total stress
Lay.	0.0.		<p>4.612 4.612 + 4.612 4.612</p>	<p>0.123 0.123</p>	<p>4.499 4.735 + 4.735 4.735</p>
Lam.	50		<p>4.358 4.358 + 4.358 4.358</p>	<p>1.026 1.026</p>	<p>5.384 3.232 + 3.332 5.384</p>
Lam.	100		<p>3.871 3.871 + 3.871 3.871</p>	<p>1.541 1.572</p>	<p>5.412 2.299 + 2.33 5.443</p>
Lam.	130		<p>3.6 3.6 + 3.6 3.6</p>	<p>1.7 1.722</p>	<p>5.3 1.878 + 1.9 5.322</p>
Mon.			<p>6.265 6.265</p>	<p>0.032 0.032</p>	<p>6.233 6.297</p>

**Table 4.** Stress distribution in the y-direction through the cross-section at the center of monolithic, layered and laminated plates ( $q = 0.04 \text{ N/cm}^2$ ).

Case	$G_1$ $\text{N/cm}^2$	Section	Stresses in y-direction ( $\text{kN/cm}^2$ )		
			Bending stress	Membrane stress	Total stress
Lay.	0.0.				
Lam.	50				
Lam.	100				
Lam.	130				
Mon.					

Table 5. Stress distribution in the y-direction through the cross-section at the center of monolithic, layered and laminated plates ( $q = 1.2 \text{ N/cm}^2$ ).

Case	$G_1$ N/cm <sup>2</sup>	Section	Stresses in y-direction (kN / cm <sup>2</sup> )		
			Bending stress	Membrane stress	Total stress
Lay.	0.0.				
Lam.	50				
Lam.	100				
Lam.	130				
Mon.					

Figures (7a-7d) show the deflection at the plate center versus the applied load for different values of the spring coefficients  $K_m$  and  $K_h$ . As can be seen both  $K_m$  and  $K_h$  have a significant effect on the deflection of the plate. Also, increasing  $K_m$  reduces the effect of  $K_h$ . Meanwhile increasing  $K_h$  reduces the effect of  $K_m$ .

### Example 2

The purpose of this example is to study the effect of the interlayer shear modulus  $G_I$  on the stress distribution through the plate thickness. The dimensions and properties of the unit are as follows:

Size of the unit	$a = 50 \text{ cm}$
	$b = 100 \text{ cm}$
Thickness of each plate	$h_1 = h_2 = 0.25 \text{ cm}$
Modulus of elasticity of glass	$E = 6.9 \times 10^6 \text{ N/cm}^2$
Poisson's ratio of Glass	$\nu = 0.22$
Interlayer thickness (if any)	$t = 0.075 \text{ cm}$
Out-of-plane spring coefficient	$K_y = 10^{20} \text{ N/cm}^2$
Rotational spring coefficient	$K_m = 0$
In-plane spring coefficient	$K_h = 0$

Tables (2) through (5) show the stress distribution through the thickness in the  $x$ - and  $y$ - directions at the plate center. This stress distribution is shown at load levels of 0.04 and  $1.2 \text{ N/cm}^2$  and at different values of  $G_I$  (0, 50, 100 and  $130 \text{ N/cm}^2$ ). The following conclusions can be obtained from the examination of these tables:

- 1- At small load level ( $q = 0.04 \text{ N/cm}^2$ , i.e., linear behavior) there is only bending stress at the center of the monolithic plate and the layered unit. However, at high load level ( $q = 1.2 \text{ N/cm}^2$ , i.e., nonlinear behavior) there is also membrane stress due to large deflection.
- 2- The bending and membrane stresses in the top plate of the layered unit with equal plate thicknesses are equal to those of the bottom plate.
- 3- For a laminated unit subjected to small load level ( $q = 0.04 \text{ N/cm}^2$ ), no direct membrane stress exists. Here, the lateral load is resisted by bending action in addition to the shear forces transferred by the interlayer. These shear forces cause normal compressive stress in the middle surface of the top plate and normal tensile stress in the middle surface of the bottom plate. These normal stresses are constant through the thickness of each plate

and are named here as "indirect membrane stresses." The moment of resistance of the unit in this case (linear stage) is the sum of the moments resisted by each plate in addition to the couple caused by the compressive and tensile forces in the top and bottom plate; respectively.

4- For a laminated unit subjected to high load ( $q = 1.2 \text{ N/cm}^2$ ), the total membrane stress is the sum of the "indirect membrane stress" discussed above and the "direct membrane stresses" due to large deflection. Here, the bottom plate is subjected to tensile membrane stress; however, the top plate may be subjected to compressive or tensile membrane stress according to the ratio of the "indirect membrane stress" which is compression and the "direct membrane stress" which is tension.

- 5- As the shear modulus of the interlayer increases, the unit becomes more stiffer, and the total stress distribution approaches that of a monolithic plate.
- 6- The membrane stress in the short direction of a rectangular plate having  $b = 2a$  is very small compared to that in the long direction. However, the bending stress in the short direction is larger than that in the long direction.

### CONCLUSIONS

In addition to the above conclusions obtained in example 2, the following conclusions can be reached from the present research:

- 1- The present model is a useful tool for the nonlinear analysis of thin laminated units resting on elastic supports.
- 2- The model successfully simulates the layered unit by equating the shear modulus and thickness of the interlayer to zeros.
- 3- Finer finite difference meshes lead to faster convergence through load steps, and higher load levels can be analyzed than in the cases of coarse meshes.
- 4- The spring coefficients  $K_m$  and  $K_h$  have a significant effect on the deflection and hence on the stresses of the laminated unit.
- 5- At high values of  $K_m$  (exceeding about  $10^5 \text{ N/cm}^2$ ) the effect of  $K_h$  on the unit deformation is negligible.

negligible for the examples cited here. Also, at high values of  $K_h$  (exceeding about  $10^5 \text{ N/cm}^2$ ), the effect of  $K_m$  on the unit deformations is negligible.

## REFERENCES

- [1] von Karman, Th., "Encyklopadie der Mathematischen Wissenschaften," Vol. IV, 1910.
- [2] Hoff, N.J. and Mautner, S.E., "Bending and Buckling of Sandwich Beams," *Journal of Aeronautic Science*, Vol. 15, No. 12, pp. 707-720, December, 1948.
- [3] Hoff, N.J., "Bending and Buckling of Sandwich Beams," National Advisory Committee for Aeronautics, Technical Note 2225, November, 1950.
- [4] Reissner, E., "Finite Deflections of Sandwich Plates," *Journal of Aeronautic Science*, Vol. 15, No. 7, pp 435-440, July, 1948.
- [5] Wang, C.T., "Principle and Application of Complementary Energy Method for Thin Homogeneous and Sandwich Plates and Shells with Finite Deflections," NACA TN 2620, 1952.
- [6] Hooper, J.A., "On the Bending of Architectural Laminated Glass," *International Journal of Mechanical Science* (Great Britain), Vol. 15, pp. 309-323, 1973.
- [7] Behr, R.A., Minor, J.E., Linden, M.P. and Vallabhan, C.V.G., "Laminated Glass Units Under Uniform Lateral Pressure," *Journal of Structural Engineering*, ASCE, 111 (5), pp. 1037-1050, 1985.
- [8] Reznik, P.L. and Minor, J.E., "Failure Strengths of Laminated Glass Units," Glass Research and Testing Laboratory, Texas Tech University, Lubbock, Texas, 1986.
- [9] Linden, M.P., Minor, J.E., Behr, R.A. and Vallabhan, C.V.G., "Experimental Study of Laterally Loaded Laminated Glass Plates," Glass Research and Testing Laboratory, Texas Tech University, Lubbock, Texas, 1988.
- [10] Basic/National Building Code, 9th Ed., Building Officials and Code Administrators Int., Inc. (BOCA), Homewood, III, 1984.
- [11] Standard Building Code, Southern Building Code Congress Int. (SBCCI), Birmingham, Ala., 1986.
- [12] Uniform Building Code, Int. Conf. of Building Officials (ICBO), Whittier, Calif, 1985.
- [13] Das, Y.C. and Vallabhan, C.V.G., "A Mathematical Model for Nonlinear Stress Analysis of Sandwich Plate Units, Mathematical Comput. Modelling, Vol. 11, pp. 713-719, 1988.
- [14] Vallabhan, C.V.G., Das, Y.C. and Magdi, M., "A Mathematical Model for Analysis of Laminated Glass Units," *Proc., ASCE Specialty Conf. of Advanced Composites in Civil Engineering Structures*, Las Vegas, Nevada, 1991.
- [15] Sakr, M.A-K., "Behavior and Ultimate Strength of Elastically Supported Laminated Plates Under Lateral Load," M.Sc. Thesis, Civil Engng. Dept., Faculty of Engng., Menofia Univ., 1993.